Interaction between the transferrin protein and plutonium (and thorium), what's new ?

Cyril Zurita, Satoru Tsushima, Pier Lorenzo Solari, Denis Menut, Sandrine Dourdain, Aurélie Jeanson, Gaëlle Creff, Christophe den Auwer

Interaction between the transferrin protein and plutonium (and thorium), what's new ?

Cyril Zurita[a], Satoru Tsushima[b,e], Pier Lorenzo Solari[c], Denis Menut[c], Sandrine Dourdain[d], Aurélie Jeanson[a], Gaëlle Creff[a], Christophe Den Auwer*[a]

[a] Dr. Cyril Zurita, Dr. Aurélie Jeanson, Asst. Prof. Gaëlle Creff, Prof. Christophe Den Auwer,
Université Côte d'Azur, CNRS, Institut de Chimie de Nice,
06108 Nice, France
E-mail: christophe.denauwer@univ-cotedazur.fr ; gaelle.creff@univ-cotedazur.fr

[b] Prof. Satoru Tsushima
Institute of Resource Ecology, Helmholtz-Zentrum Dresden-Rossendorf (HZDR),
01328 Dresden, Germany.
E-mail: s.tsushima@hzdr.de

[c] Dr. Pier Lorenzo Solari, Dr. Denis Menut
Synchrotron SOLEIL, L'Orme des Merisiers, ,
F91190 Saint Aubin, France
E-mail: pier-lorenzo.solari@synch)rotron-soleil.fr ; denis.menut@synchrotron-soleil.fr

[d] Dr. Sandrine Dourdain
ICSM, Université de Montpellier, CEA, CNRS, ENSCM, Marcoule, France.
E-mail : sandrine.dourdain@cea.fr

[e] Internationnal Research Frontiers Initiative, Institute of Innovative Research, Tokyo Institute of Technology, Meguro, 152-8550, Tokyo, Japan

Abstract:
Transferrin (Tf) is a glycoprotein that transports iron from the serum to the various organs. Several studies have highlighted that Tf can interact with metals other than Fe(III), including actinides that are chemical and radiological toxics. We propose here to report on the behavior of Th(IV) and Pu(IV) in comparison with Fe(III) upon Tf complexation. We considered UV-Vis and IR data of the M_2Tf complex (M = Fe, Th, Pu) and combined experimental EXAFS data with MD models. EXAFS data of the first M-O coordination sphere are consistent with the MD model considering 1 synergistic carbonate. Further EXAFS data analysis strongly suggests that contamination by Th/Pu colloids seems to occur upon Tf complexation, but it seems limited. SAXS data have also been recorded for all complexes and also after the addition of Deferoxamine-B (DFOB) in the medium. The Rg values are very close for apoTf, ThTf and PuTf, but slightly larger than for holoTf. Data suggest that the structure of the protein is more ellipsoidal than spherical, with a flattened oblate form. From this data, the following order of conformation size might be considered : holoTf < M_2Tf (M = Th, Pu) < apoTf < M_2Tf-DFOB (M = Fe, Th, Pu).

Introduction

Since the discovery of nuclear fission in 1938, the nuclear industry in both the civil and military sectors has dramatically expanded, most notably in the Northern Hemisphere. These developments have given rise to new geostrategic, geopolitical and environmental challenges that also lead to concerns regarding security, the environment, and indeed the entire biosphere. Nuclear energy has also become a key strategy for many nations, who must therefore develop policies that mitigate these potential dangers. It is well known that fission products, activation products and actinide elements associated with nuclear fuel can be chemically and radiologically toxic if accidentally released into the environment.[1] Of these, actinides are the heaviest elements that may be involved and have no essential biological function. They are thus transported in the organism towards target organs, and are retained or excreted, while expressing their dual radioactive and heavy metal toxicity.[2] The main routes of contamination for actinides during internal exposure are inhalation of aerosols (pulmonary route), ingestion (gastrointestinal), and penetration through an open wound (subcutaneous) and skin.

In vivo, Pu is mainly present in the +IV oxidation state.[3] It is a hard acid cation on the Pearson scale, it has a large coordination number (8-12) and a large propensity for hydrolysis.[4] The intake of Pu therefore poses considerable health risks if contamination occurs. Early studies on Pu accumulation in rats have provided evidence of the importance of the metal speciation and have described its biokinetic characteristics.[5,6] Pu(IV) injection has shown that its distribution is similar in all animal species studied (mammals), with very little excreted in the urine.[7] After ingestion, post-mortem radiometry in humans has shown that 90% of the Pu activity in extra pulmonary sites is accumulated in the liver and skeleton.[8,9] Furthermore, the percentage deposited in the skeleton increases with time. In various mammals species, 85% of the injected Pu(IV) is deposited in bone and liver, with a bone-liver distribution varying according to speciation.[2]

In the absence of steric constraints, Pu^{4+} tends to form complexes as stable as those of the first-row trivalent transition metals, especially Fe^{3+} due to their comparable charge-radius ratios (Fe(III) = 0,645 Å, CN = 6 ; Pu(IV) = 0,96 Å, CN = 8 to 10) and have a high affinity for carboxylate functions.[10] In mammals, the large majority of Fe is associated with the hemoglobin protein, allowing the transport of oxygen in our organism.[11]. The small amount of Fe that remains can also interact with the transferrin protein (Tf) to be

transported from the serum to the cells.[12] Previous reports have suggested that Tf is also a possible target of Pu that would be transported into the cells.[13,14 15]] Tf, once bound to Pu, could cross the cell barrier (endocytosis) and thus could enter the cell. Jensen *et al.* have proposed a mechanism for Pu-Tf recognition by cells in which the proposed model involves a FePuTf mixture, with Pu bound to the C lobe and Fe to the N lobe.[16] This is why the interaction of Pu(IV) with Tf would give key indications on its possible internalization mechanism in the cells.

Tf is a glycoprotein with a molecular weight of around 80 kDa. The role of this protein is to transport iron from the serum to the various organs.[17,18] Tf consists of a single polypeptide chain of 670-700 amino acids and has two lobes, named N and C connected by a short bridge.[19] These two lobes have a similar but not identical affinity for metal cations.[20] Each of the two lobes of the protein contain a metal binding site that can bind one ferric ion.[21,22] The bio-distribution of the different Tf complexes is 27% of Fe_2Tf (also called holoTf), 23% of Fe_NTf, 10% of Fe_CTf and 40% apoTf (Tf with no metal).[23] Each Fe(III) atom binds similarly one lobe of the protein. The coordination of Fe(III) in each lobe involves four amino acids consisting of two tyrosine, one histidine and one aspartate residue.[24,25] It also binds with a synergistic anion, usually a bicarbonate or carbonate anion to complete the Fe coordination sphere. The 4 amino acids and carbonate anion fulfill the Fe coordination sphere (CN = 6) leading to the lobe closure.[26] The Fe_2Tf complex (pK_D = 20.9 ± 0.6)[22] is thus in the appropriate closed conformation to be recognized by the transferrin receptor protein (RTf) on the cell surface and to cross the cell membrane.[27]

Several studies have highlighted that Tf can interact with metals other than Fe(III) such as titanium, vanadium, chromium, ruthenium and bismuth.[15] Other metals including certain actinides can also interact with Tf.[28] For instance, Tf binds strongly with Pu(IV) with a reported conditional constant pK_D = 21.75 ± 0.75 comparable to that of Fe(III).[29]

In vivo, the exact conformation of complexed M_nTf (M = metal, n = 1,2) and the occurrence of this conformation is often not known. A previous report by Jensen *et al.* has shown that the interaction of the Pu_2Tf complex with the transmembrane receptor RTf can only occur in presence of Fe within the protein to form a mono-plutonium mono-iron Tf complex in the PC12 cells.[15] In the active form of the Pu-loaded Tf, *i.e.* a conformation that is able to bind to RTf and cross the cell membrane barrier, Pu(IV) is complexed to the binding site of the C-lobe of the protein, and Fe(III) to the N-lobe of the protein (Pu_CFe_NTf). According to this report, all other forms of Pu_2Tf and PuFeTf complexes that may exist *in vivo* do not have a suitable conformation to subsequently bind with the RTf receptor. The slight binding differences between the two lobes of Tf therefore turns off its complexation with RTf and by extension, the cellular uptake of Pu.[16,25]

In the present report we propose to revisit the interaction of Pu(IV) as well as Th(IV) with Tf with a methodology that addresses the conformational change of the protein after complexation by both metals. ^{232}Th has been used here as a surrogate of ^{239}Pu for the test experiments (it is less radioactive) but also to allow a comparison between the two actinides. Th(IV) and Pu(IV) local environments in M_2Tf (M = Th, Pu) complexes were first explored with XAS (*X-ray Absorption Spectroscopy*) complemented with IR (*Infra-Red*) and spectrophotometry. A macromolecular model obtained with MD (*Molecular Dynamic*) calculations allowed us to identify which amino acids are involved in this interaction and to understand the change in the overall conformation of the protein after complexation. MD calculations were also used to interpret structural information obtained from SAXS (*Small Angle X-ray Scattering*) data on M_2Tf and holoTf complexes compared to apoTf. Based on these results, we propose a model of complexation and of conformation between Pu/Th and Tf with respect to Fe.

Results and Discussion

To avoid hydrolysis at physiological pH, Th(IV) and Pu(IV) were protected with carbonate anions which are found in the serum at 22 mM to 28 mM levels. The limit complexes $M^{IV}(CO_3)_5^{6-}$ (M = Th, Pu) were prepared and used as stock An solutions (see experimental section). In the text that follows, the carbonate anions will be omitted from the notation M_2Tf (M = Th, Pu) for clarity but are nevertheless present. The notations apoTf and holoTf are related to the commercial Tf without and with iron respectively.

Thorium, Plutonium complexation, spectrophotometry

The complexation of Tf with Pu(IV) in presence of carbonates (Pu_2Tf) has been monitored by spectrophotometry (Figure 1) and compared to the spectra of apoTf and holoTf. The same comparison has been performed for the complexation of Tf with Th(IV) in presence of carbonates (Th_2Tf). All spectra have been normalized to the absorption band at 280 nm. This band is characteristic of $\pi \rightarrow \pi^*$ transitions in the protein, and mainly due to the tyrosine and tryptophan chromophore groups.[30,31] The spectrum of holoTf shows an absorbance band in the range 463-472 nm attributable to a tyrosyl phenolate (p_π) → Fe(III) (d_{π^*}) charge transfer transition.[32] The spectra of Th_2Tf and Pu_2Tf are different from each other but also from the spectrum of holoTf and apoTf. Furthermore, in the 300-375 nm range, the presence of an absorption band not observed in the apoTf spectrum may be a signature of the formation of a Tf complex with the different metals.[33,34]

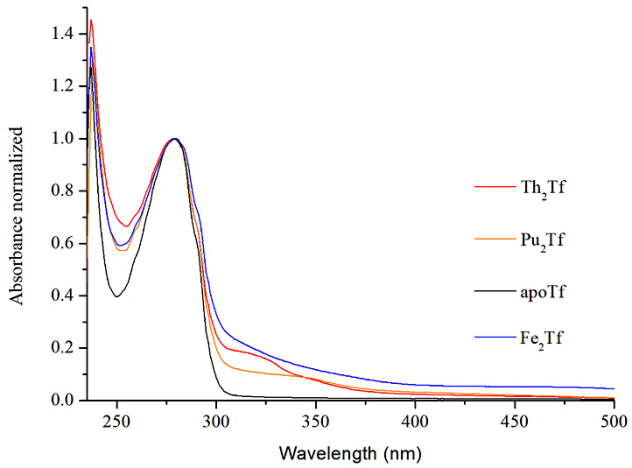

Figure 1: UV-Visible spectroscopy comparison of Th_2Tf (red line), Pu_2Tf (orange line), holoTf (blue line) and apoTf (black line).

Thorium, Plutonium complexation, Infrared spectroscopy

In order to obtain a first description of the chemical environment of the metal within the Tf complex, IR spectra were recorded with Fe(III), Th(IV) and Pu(IV).

Figure S1 of SI shows a comparison between the spectra of apoTf (black line), holoTf (blue line), Th_2Tf complex (red line) and Pu_2Tf complex (orange line). Note that all the Tf complexes were micro-filtrated at 3 kDa and then washed to remove the excess of the synergic anion (see experimental section). The IR transmission spectra were normalized to the amide II band at 1550 cm^{-1} as this band is less strongly influenced by complexation with metals than the amide I band.[35] Figure S1 of SI shows that the spectrum of apoTf is very similar to that of holoTf. The spectra of M_2Tf (M = Th, Pu) have a similar (although not identical) signal in the region 1450 - 1200 cm^{-1} that is however little different from both spectra of holo and apoTf. Note that the spectrum of Pu_2Tf was recorded using a specific ATR module, which makes the acquisition conditions different from the other three spectra (see experimental section). This first examination of the spectra shows that in our working conditions there is no evidence of protein degradation. Indeed, the structure of the amide I band is affected by the presence of the metals evidencing modifications in the protein conformation upon complexation. The large band centered at 1366 cm^{-1} on the two M_2Tf spectra could be attributed to the antisymmetric ν_3 vibration of carbonate groups present in the sample.

Thorium, Plutonium local environments, X-ray Absorption Spectroscopy

To cast light on the complexation site of Pu/Th in M_2Tf complexes (M = Th, Pu), XAS data at the cation L_{III} edge have been recorded in the EXAFS (Extended X-ray Absorption Fine Structure) regime. A first comparative observation of the XANES part of the spectra with MO_2 oxide references (spectra not shown) confirms the +IV oxidation state, not surprisingly. A qualitative comparison between the EXAFS spectra of Th_2Tf and Pu_2Tf in Figure 2 indicates that the local environment in both protein complexes is very similar. Additional comparison with the $M^{IV}(CO_3)_5^{6-}$ (M = Th, Pu) complexes at pH 10 shows unambiguously that the EXAFS signature of the M_2Tf complexes in our working conditions is different from the pure carbonate complexes signature. A shift in low k values and a modification of the wave shape are visible in Figure 2.

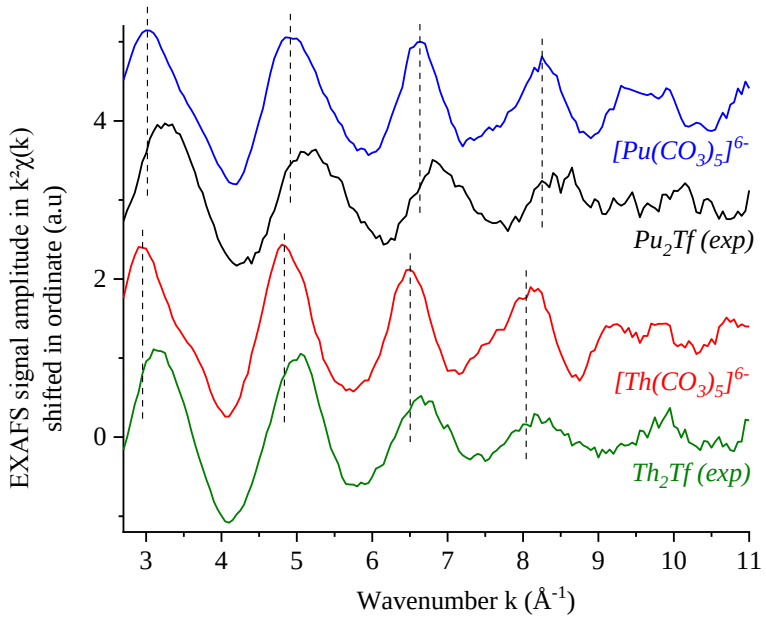

Figure 2 : Comparison of experimental EXAFS spectra in $k^2\chi(k)$ of Pu_2Tf with $[Pu(CO_3)_5]^{6-}$ complex and Th_2Tf with $[Th(CO_3)_5]^{6-}$ complex.

In order to adjust the EXAFS data with *ad hoc* structural models and attempt to go beyond a description with averaged scattering shells, models of Pu_2Tf were created by MD calculation. To realize these models, a Ce(IV)- transferrin structure (PDB reference 1FCK) was used as a starting point.[36] Ce(IV) is an interesting element since it can be considered as a non-radioactive analogue of Pu(IV) (Ce is the only lanthanide stable at oxidation state +IV in aqueous solution). In these calculations, Ce(IV) has been substituted by Pu(IV) while varying the number of metal-interacting carbonate groups in each lobe. These calculations were performed for 100 ns mimicking physiological pH (pH 7.4) by adjusting the protonation states. Each model has a different carbonate stoichiometry with respect to Pu, ranging from 0 to 3 (a stoichiometry of 4 or above lead to instabilities and unrealistic results), reflecting that several carbonate anions can bind to the metal within the Tf binding site. Carbonate anions are also known to bind through H-bonding to the amino acids of the protein to close the complexation site.[37] On the other hand, in the absence of any carbonate (simulation with 0 carbonate) the Pu_2Tf complex was found to be unstable, to stay in a folded state and the lobe opened up in the middle of the simulation. Therefore, the result with 0 carbonate is excluded from further discussion. The three models (1-3 carbonates) are compared to the crystallographic structure of Fe_2Tf (PDB 1N04) and Ce_2Tf (PDB 1FCK) in Figure S2 and Table S1 of SI. In the N lobe, Pu is bound notably to Asp60 as in the case of the 1FCK (Ce) and 1N04 (Fe) structures. In the C lobe, Pu is bound to Asp395 residue as in Ce_2Tf and Fe_2Tf models (see Table S1 of SI).[36]

More precisely, in the Pu_2Tf model with a carbonate in each lobe, denoted Pu_2Tf(*1carb*), although the amino acids interacting with the metal are different, the interaction mode is close to that of 1FCK and 1N04 crystallographic structures. In the Pu_2Tf models with two or three carbonates, named Pu_2Tf(*2carb*) and Pu_2Tf(*3carb*), respectively, a decrease in the number of amino acids bound to the metal is observed compared to the Pu_2Tf(*1carb*), 1FCK and 1N04 models. This decrease, in particular for *3carb* can be explained by the increase of the number of carbonates interacting with Pu which induces the repulsion of the amino acids of the protein making this interaction with Pu(IV) more difficult. Overall, the molecular models reveal that local environments in each lobe around Pu that are not very similar to that of natural Fe. However, we note in the different models the presence of residues of glutamate, serine, alanine, proline or threonine which do not intervene in the holoTf. On the other hand, tyrosine and histidine residues, present in the case of Fe(III), do not appear in the close environment of the Pu(IV) atoms. However, the presence of the same aspartate residue in each of these lobes indicates that Pu(IV) is indeed suggested in the same site as Fe(III). Because the sidechain of tyrosine has a large pKa value (> 10), in the MD simulations, they were all assumed to be protonated. They may get deprotonated upon coordination to metal as pointed out previously.[38] Deprotonation occurs only after the coordination of Tyrosine, and if we assume it to be deprotonated from the beginning, it would certainly add bias to the calculations. Therefore we restricted ourself to the use of protonated tyrosine. Overall, direct coordination of tyrosine to Pu was rarely observed during the simulation (exception for one Tyr coordination in C-Lobe for two carbonate system), though the tyrosine involved in Fe(III)-binding always remained in the vicinity of Pu(IV). Therefore, despite that Pu(IV)-Tf does not share the same metal coordination environment as Ce(IV)-Tf, there is hardly any conformational change upon Ce-to-Pu substitution.

When comparing the calculated EXAFS spectra for each lobe N and C for a given model (see Figure S3 of SI), the presence of several carbonates greatly modifies the environment around Pu(IV). In order for it to be compared more precisely with the experimental spectrum of Pu_2Tf, the average of the calculated spectra for the two lobes for each model was calculated and is presented in Figure 3. It compares the experimental EXAFS spectra of Pu_2Tf, $Pu(CO_3)_5^{6-}$ and the calculated spectra for each model (both lobes averaged).

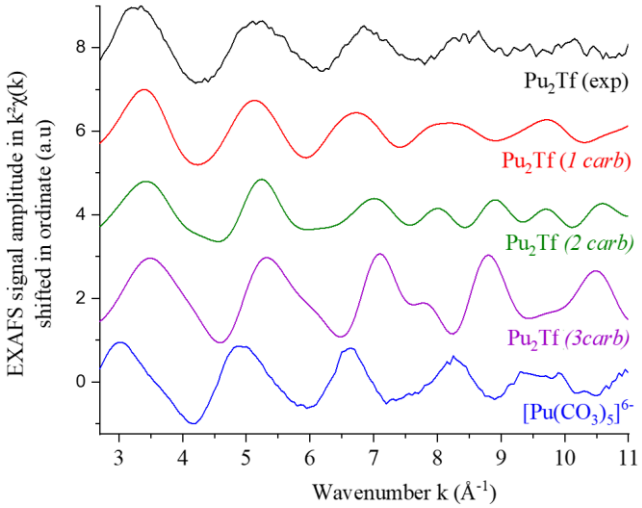

Figure 3: Comparison of theoretical EXAFS spectra in $k^2\chi(k)$ of the different models: Pu_2Tf (1 carb) model (red line), Pu_2Tf (2 carb) model (green line) and Pu_2Tf (3 carb) model (purple line) with the experimental spectrum of Pu_2Tf (top black line) and of $[Pu(CO_3)_5]^{6-}$ complex (bottom blue line).

Table 1. Best-fit structural parameters obtained from the fit of EXAFS Pu_2Tf (exp), Th_2Tf (exp) data. Comparison with $[Th(CO_3)_5]^{6-}$ and $[Pu(CO_3)_5]^{6-}$ from ref [39]. σ^2 is the Debye Waller factor of the considered diffusion path. $S0^2$ is the global amplitude factor, ΔE0 is the energy threshold, Factor-R is the fit factor in % and Factor-Q is the quality factor (reduced χ^2) of the fit. The uncertainties in brackets.

Sample	1st shell	2nd shell	S0² ΔE0 (eV) Q factor R-factor
Pu_2Tf (exp)	2.8(3) O at 2.21(1) Å σ^2 = 0.0030 Å² 6.2(8) O at 2.36(1) Å σ^2 = 0.0030 Å²	3.1(11) C at 3.23(2) Å σ^2 = 0.0034 Å² 0.8(2) Pu at 3.85(2) Å σ^2 = 0.0040 Å²	1.0 3.32 5.7 1.1%
$Pu(CO_3)_5^{6-}$	10.2(4) O at 2.44(2) Å	5.1(4) C at 2.88(1) Å	from ref 39
Th_2Tf (exp)	2.9(9) O at 2.27(1) Å σ^2 = 0.0057 Å² 9.6(9) O at 2.43(3) Å σ^2 = 0.0057 Å²	2.9 (10) C at 3.02(13) Å σ^2 = 0.0055 Å² 0.7(5) Th at 3.90(3) Å σ^2 = 0.005* Å²	1.0 1.79 12.7 1.3%
$Th(CO_3)_5^{6-}$	10.8(4) O at 2.50(8) Å	5.4(4) C at 2.96(9) Å	from ref 39

The calculated EXAFS spectrum of Pu_2Tf(1carb) is qualitatively close to the experimental spectrum of Pu_2Tf in Figure 3. On the contrary, the model with three carbonates shows significant differences and does not resemble any of the experimental spectra, neither $Pu(CO_3)_5^{6-}$ nor Pu_2Tf(exp).

The spectrum of Pu_2Tf(*2carb*) shows an intermediate behavior. The difference between the calculated spectra and that of the experiment may be estimated point by point according to the formula: $|\Delta k| = \chi(k)$ Pu_2Tf (*ncarb*) - $\chi(k)$ Pu_2Tf (exp). This average difference between the model signal and the experimental signal is only indicative over the entire spectra but it corroborates the qualitative comparison : 18 % for Pu_2Tf (*1carb*); 22 % for Pu_2Tf (*2carb*) and 44 % for the Pu_2Tf(*3carb*). Clearly, the distinction between both models *1carb* and *2carb* is difficult to make at this stage, but *3carb* can be excluded (similarly *0carb* has been excluded). In order to use a model as simple as possible and also to match with the holoTf, the 1carb model was chosen and is shown in Figure 4. For comparison, models Pu_2Tf (*1carb*) and Pu_2Tf (*2carb*) are presented in Table S1 of SI). Accordingly, the N-lobe site of PuTf(*1carb*) was chosen to generate the scattering paths for EXAFS data fitting (lobe C of this model was not selected as shown in Figure S4 of SI).

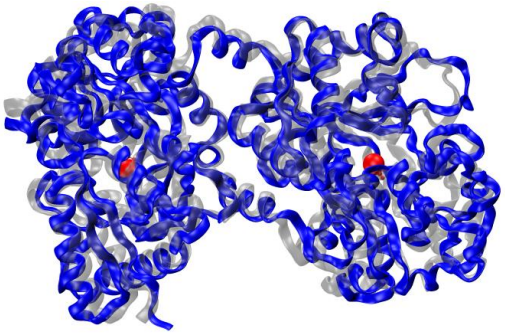

Figure 4 : Superposition of the PDB structure of Ce_2Tf (1FCK, grey) with the structure of Pu_2Tf(*1carb*) (blue) calculated by molecular dynamics. In red are the 2 metallic complexation sites of the N- and C-lobes.

The best fit parameters of the EXAFS spectra of Pu_2Tf (exp) and Th_2Tf (exp) (Pu has been replaced by Th in the model) are shown in Table 1 The best fit data for Pu_2Tf reveals a first shell composed of 2.8(3) and 6.2(8) O with distances of 2.21(1) Å and 2.36(1) Å. Comparison to the best fit data of the $Pu(CO_3)_5^{6-}$ reference shows a significant shrinking of the O first coordination sphere (the same remark will be valid for Th_2Tf compared to $Th(CO_3)_5^{6-}$).[39] In the Pu_2Tf(*1carb*) model, oxygens are present at distances spanning from 2.20 to 2.68 Å, very disperse. Figure S5 of SI shows the radial distribution of the 20 oxygen atoms from lobes N and C in Pu_2Tf(*1carb*) model. The EXAFS data represented by an arrow on the graph of Figure S5 are very consistent with the model, although on the shorter side of the dispersion. The second shell of carbon atoms in the model contains two distinct layers of 8 carbon atoms from lobes N and C, but only the first set (from 2.7 to 3.1 Å) is likely to be EXAFS sensitive. The EXAFS data could indeed be fitted with one layer of C atoms and attempts to add a second layer at a larger distance as in the model did not affect the fit. The experimental fitted average distance is about 0.2 Å larger than in the model, suggesting a significant difference in the amino acid conformation. Attempts to reduce this distance led to a significantly degraded fit. Similarly, very similar Th-O distances were obtained for Th_2Tf, although slightly larger because of the larger ionic size of Th^{4+} compared to Pu^{4+}. On the other hand, the average Th…C distance is significantly smaller than for Pu and in better agreement with the Pu_2Tf(*1carb*) model. At this point we have no explanation for these discrepancies in the M…C coordination sphere except that significant second sphere rearrangements from the amino acid carbon atoms compared to the static model are not surprising.

As shown in Figure S6 of SI, an additional contribution at R+Φ = 3.6 Å is not reproduced well by the fit. This contribution indicates that another interaction is visible and could signal a Th/Pu...Th/Pu interaction as in colloidal Pu(IV) (localized around 3.8 Å in R-space).[40] This contribution was filtered and could be fitted with a path of Pu...Pu scattering in the case of Pu_2Tf. The Pu...Pu distance at 3.85(2) Å (see Table 1) is consistent with the distance of a colloidal plutonium compound.[40] The same observation was made for Th_2Tf. Since this contribution is not present in the fitting of $Th/Pu(CO_3)_5^{6-}$ it suggests the formation of a small quantity of colloids in our conditions for Tf complexation. The small amplitude value associated with this scattering path in Table 1 strongly suggests negligeable colloidal contamination as discussed in the Discussion section.

Transferrin conformation upon Pu/Th complexation

Additional SAXS (Small Angle X-ray Scattering) data were acquired to cast light on the tertiary structures of the M_2Tf (M = Fe, Th, Pu) complexes. Furthermore, we also investigated the influence of a competing ligand in order to observe the effect of complexation and decomplexation on the Tf conformation. Deferoxamine-B (DFOB) siderophore was chosen because it is known to interact strongly with Fe(III) ($\beta_{1,1}$ = 31.0 ± 0.3 in KCl 0,1 M) and Pu(IV) ($\beta_{1,1}$ = 35.8 ± 0.9 in $NaNO_3$ 0.1 M).[41,42] Thus, the addition of DFOB to Pu_2Tf may induce a total or partial decomplexation of Pu or the formation of a Pu_2Tf-DFOB ternary complex.

Sample	c	a	Fitting error χ^2

apoTf	16.1 ± 0.1	45.3 ± 0.3	5.10^{-6}
holoTf	13.9 ± 0.1	43.8 ± 0.2	9.10^{-6}
Pu_2Tf	15.5 ± 0.2	45.9 ± 0.1	3.10^{-6}
Pu_2Tf-DFOB	16.3 ± 0.2	47.1 ± 0.3	6.10^{-6}

The UV-Vis spectrum of DFOB measured in the presence of Pu_2Tf complex (blue line), is plotted in Figure S7 and compared to the spectra of apoTf (black line), free DFOB molecule (orange line), Pu_2Tf (red line) and of a Pu-DFOB complex (purple line). All spectra are normalized to the absorption band at 280 nm. Figure S7 indicates that the addition of 10 DFOB to Pu_2Tf (1:5 Pu:DFOB ratio) does not lead to the total decomplexation of the Pu(IV) bound to the protein. The spectrum is still dominated by the signal of Tf while the band of Pu_2Tf around 340 nm is clearly disappearing. Although it is difficult to draw any further conclusions, one may hypothesize that DFOB is either partially decomplexing Pu from Tf or forming a ternary complex Pu_2Tf-DFOB.

Table 2. Best fits results of SAXS spectra with an oblate structure. a: is the longer dimension called equatorial radius (in Å) c: is the smaller dimension called polar radius (in Å).

The SAXS spectra of Pu_2Tf, Th_2Tf, holoTf, apoTf, Th_2Tf-DFOB, Pu_2Tf-DFOB and holoTf-DFOB are shown in Figure 5 and standard deviations are provided in Table S2 of SI. The spectra of the different complexes are compared with the spectrum of the pure apoTf (see SI paragraph 3 for details).

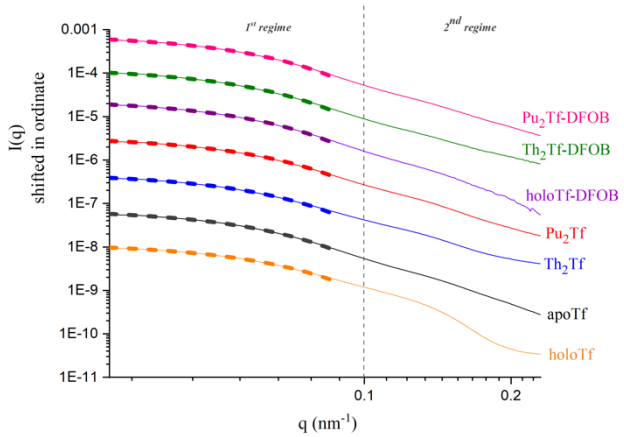

Figure 5: Scattering spectra of apoTf, holoTf M_2Tf, holoTf-DFOB and M_2Tf-DFOB complexes (solid lines) at physiological pH (M = Th, Pu) and their Guinier fits (dotted lines).

The shape of these spectra shows a rise of scattering signal towards the small Q vectors. This increase of signal is attributed to the scattering of the protein. Two decreases of intensity can moreover be observed, indicating two distinct dimensions in the protein structure. The first, located between 0.03 nm^{-1} to 0.09 nm^{-1}, and the second, between 0.1 nm^{-1} and 0.22 nm^{-1}, are characteristic of a large and a small dimension of the protein, respectively. They are denoted as 1st and 2nd regime in Figure 5. It can be noticed that the first drop of intensity appears similar for all the complexes, while the second shows distinct behaviors depending on the complex. For instance, the decrease in intensity of the spectrum of holoTf is clearer than that of the spectrum of apoTf, while spectra obtained for Th_2Tf and Pu_2Tf also show these two drops of intensity but are more attenuated than for holoTf. These first

indications confirm that the complexation of the protein influences its conformation. The addition of DFOB in the medium induces a significant modification of the SAXS spectra. Structural changes upon complexation are therefore detectable with SAXS.
In order to interpret quantitatively these changes, gyration radii were first fitted with the Guinier approximation applied on the 1st regime of the curves (see Table S3 of SI). The radii of gyration determined in this work are compared to the literature as well as to the radii of gyration of the different models of Pu_2Tf, with 1,2 or 3 carbonates, also in this work. First, we observe that the holoTf complex adopts a smaller conformation than the apoTf, with a conformational difference of 1.1 ± 0.2 Å. For instance, the radii of gyration obtained by Yajima *et al.*[43], although with a different buffer media, was greater than ours, but still had a difference of 1.0 Å between apoTf and holoTf. For Th_2Tf and Pu_2Tf complexes, the radii of gyration of Table S3 of SI are very close and comparable to that of apoTf. In their study, Jensen *et al.*[16] observed (although absolute values are different) a larger radius of gyration for Pu_2Tf than for holoTf, indicating again a different structure and thus an open conformation for Pu_2Tf. This is consistent with our results. Moreover, the radius of gyration obtained from MD simulations are close regardless of the carbonates number. Finally, the addition of DFOB to the M_2Tf (M = Th, Pu) complex increases the gyration radius. These values suggest that DFOB partially binds to the metal in interaction with transferrin, thus increasing the overall gyration radius of what would be best described as a ternary complex. In the case of holoTf (Figure 5), DFOB appears to partially interact with Fe, resulting in an increase in the gyration radius measured between holoTf and holoTf-DFOB. This increase could be explained by an opening of the protein lobes when the holoTf-DFOB ternary complex is formed. Indeed, Bellotti and Remelli also observed that DFOB does not fully decomplex the protein from Fe.[44] In our study, Pu and Th also appear to interact with DFOB, and may also form a ternary complex with the protein.
To provide a more quantitative analysis of the SAXS data, a form factor considering a non-spherical shape of the scattering objects was used. Martel *et al.* studied the structure of holoTf and showed that a flattened ellipsoid of revolution (oblate) form factor is a simple structure similar to that of this protein.[45] Two parameters were used: a polar radius c (the shortest distance) and an equatorial radius a (the longest distance). The fit of the data of holoTf, Pu_2Tf, Pu_2Tf-DFOB and apoTf complexes are shown in Figure 6. The fitted parameters of both dimensions of the protein are given in Table 2.

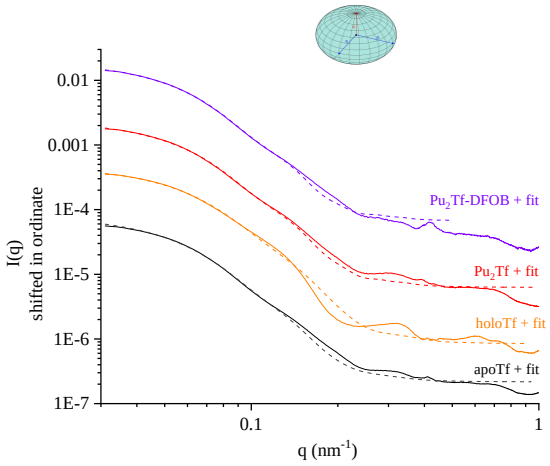

Figure 6: SAXS spectra of holoTf, Pu_2Tf, Pu_2Tf-DFOB and apoTf complexes (solid line) and their fitting by an oblate ellipsoidal structure (dotted line).

The slight structural changes between the open and closed conformations of the protein are further highlighted by these fits using the oblate structure. The polar radius c is the most affected by the conformational change of the analyzed complexes. Indeed, a decrease of this radius, from apoTf to holoTf is observed in agreement with the conformational change of the protein. Similarly, the polar radius of Pu2Tf is slightly smaller than that of apoTf, but larger than that of holoTf, which is consistent with a slight closure of the protein in the presence of Pu.
In contrast, the polar radius of the Pu_2Tf-DFOB complex is larger than that of apoTf. In comparison, the equatorial radius of the different fitted complexes is only slightly impacted by the conformational changes. Martel et al. have also analyzed the shape of human holoTf by SANS (Small Angle Neutron Diffusion) using a flattened ellipsoidal structure and obtained values of 46.6 ± 1.4 Å and 15.8 ± 3.8 Å for the equatorial and radial radii respectively.[45] In addition, they also observed that the oblate ellipsoidal structure is the best simple approximation to the shape of the Tf molecule. Our data are in good agreement with those published by Martel *et al.* and confirm the choice of this form factor.

Discussion

Models of Pu_2Tf obtained from MD calculations show that increasing the number of carbonates (from 1 to 3) interacting with Pu prevents the amino acids of the protein from entering the coordination sphere. Indeed, with 3 carbonates or higher, they seem to repel the amino acids, which end up at a distance larger than 5 Å from the metal. Furthermore, the MD model suggests that the

residues Asp 60 and Asp 395 in the N and C lobes respectively, are present in the local environment of Fe and Pu. The local environments of Fe and Pu are not seen as identical due to the presence of residues in the Pu environment that are not found in the Fe environment. This would also support the differences observed in the UV-Vis data that are very sensitive to the metal coordination sphere.

A careful comparison of these simulation data with experimental EXAFS spectra supports the presence of Th and Pu in the Fe coordination site. It also suggests that only 1 carbonate (an assumption with 2 cannot be excluded but seems less likely) is present in the local environment of Pu and Th, as is the case of Fe. Comparison of our best fit EXAFS data of Pu_2Tf can be made with data published by Jeanson *et al.* in 2010, however using NTA as the synergistic anion.[46] The parameters of the first oxygen coordination sphere are very similar (2.21 / 2.36 this work, 2.21 / 2.37 Jeanson *et al.*) but are markedly different in the second carbon sphere (3.23 this work, 3.33 / 3.47 Jeanson *et al.*). But further comparison with the present system is difficult because of the presence of NTA in Jeanson's study whose size is significantly larger than that of the carbonate and probably resulted in a rearrangement of the amino acids conformation. Finally the presence of Pu or Th atoms at a distance of 3.8 - 3.9 Å is required here for the fits. Our assumption is that a "contamination" by colloids or another type of condensed metallic cluster occurs upon Tf complexation since the metal carbonate complexes used at the start do not show any "contamination". Therefore, an estimate of this "contamination" can be made according to the structure of the colloids reported by Micheau *et al.*.[47] In this case 0.8 Pu (0.7 Th) would represent about 10% of colloidal species in our sample. During the preparation of Th/Pu_2Tf, a Th/Pu : Tf ratio of about 2.2 : 1 was used in order to saturate both lobes of the protein. The minor excess of free Th/Pu is then likely to occur in the solution. And after adjustment to physiological pH, the carbonate being no longer predominant at this pH range would not sufficiently protect the Pu against hydrolysis. Micheau *et al.* also showed that plutonium particles, obtained in an acidic medium, have a radius of gyration Rg of about 10.4 ± 0.5 Å,[47] characterized by a bend at about Q ~ 2 nm^{-1} in the SAXS data. This was not observed in all our spectra. A careful look at Jeanson's data from 2010 shows a similar contribution at R+Φ = 3.6 Å that was difficult to fit because it may have had the same origin.

Differences in the metal coordination sphere also have an impact on the potential closure of Tf after complexation. The two decreases in intensity observed on our SAXS spectra are characteristic of the Tf shape as they are also observed in the absence of Pu and in the literature.[16] Fitting the scattering spectra with a simple oblate ellipsoid model led to a good reproduction of the experimental data until Q= 0.2nm^{-1}. For higher Q range, additional oscillations were identified, which cannot be fitted with a simple form factor. The fitted data of Table 2 suggest that the Pu_2Tf complex is larger than holoTf but slightly smaller than apoTf. On the other hand, Rg values given in Table S3 of SI are very close for apoTf, ThTf and PuTf, but slightly larger than for holoTf. Furthermore, it is interesting to observe that the gyration radii of both calculated Pu_2Tf models (*1,2carbs*) are similar to each other, confirming a close or partially close conformation in both cases with Pu (absolute values of Rg must be considered with caution).

Finally, it is interesting to note that the addition of DFOB with the already existing M_2Tf complex (M = Fe, Th, Pu), favors the formation of the ternary complex M_2Tf-DFOB whatever the metal with a clear open conformation. Indeed, the radius of gyration measured for these ternary complexes is higher than that of apoTf, which seems to indicate that DFOB partially binds with the metal in the protein. In addition, these ternary complexes were also observed by UV-Vis analysis.

In conclusion, the above data complement previous literature on actinide(IV)-Tf interaction and suggest the following order of conformation size : holoTf < M_2Th (M = Th, Pu) < apoTf < M_2Tf-DFOB (M = Fe, Th, Pu). This order is in full agreement with the expected behavior of Tf as explained above.

Conclusion

The interaction between transferrin (Tf) and exogeneous metals is still an open question despite the vast literature on the subject. In this work, we proposed to further characterize the behavior of Th(IV) and Pu(IV) in comparison with Fe(III) upon Tf complexation. We first considered UV-Vis and IR data of the M_2Tf complex (M = Fe, Th, Pu) and combined experimental EXAFS data with MD models in order to better describe the metallic coordination site. In all cases, the iron coordination site is involved although MD models suggest that the local environments of Fe and Pu are not identical due to the presence of residues in the Pu environment that are not found in the Fe environment. EXAFS data of the first M-O coordination sphere are consistent with the MD model considering 1 synergistic carbonate. Further EXAFS data analysis strongly suggests that contamination by Th/Pu colloids seems to occur upon Tf complexation, but this contamination seems limited to *c.a.* 10%.

SAXS data have been recorded for all complexes and also after the addition of DFOB in the medium. The Rg values are very close for apoTf, ThTf and PuTf, but slightly larger than for holoTf. To provide a deeper quantitative analysis of the SAXS data, a form factor considering a non-spherical oblate shape of the scattering objects was considered as for holoTf. Data suggest that the structure of the protein is more ellipsoidal than spherical, with a flattened oblate form rather than an elongated ellipsoid in agreement with Martel's data on holoTf.[45] From this data, the following order of conformation size might be considered : holoTf < M_2Th (M = Th, Pu) < apoTf < M_2Tf-DFOB (M = Fe, Th, Pu). The interaction with DFOB is therefore an interesting subject for investigation as we seek means of reducing the affinity of a Pu_2Tf-DFOB ternary complex with the RTf1 transmembrane receptor, which is the entry pathway of Tf into the cell.

Experimental section

All chemicals used were of analytical grade except for the protein. Human apo-Transferrin and holo-Transferrin were purchased from *Sigma-Aldrich*. The commercial batch was dialyzed prior to use: apo-Transferrin or holo-Transferrin was placed in a 12 kDa membrane and dialyzed for 24-hours 3 times in buffer medium $5x10^{-2}$ M MES, $1.5x10^{-1}$ M NaCl, pH 7.4 ± 0.1.

Actinide (Th, Pu) stock solutions

^{239}Pu (96% 239, 4% 240) was obtained from CEA stock. $Pu(CO_3)_5^{6-}$ stock solution was prepared by mixing 120 µL of Pu(IV) at $6 x10^{-3}$ M and 120 µL of carbonate at 3 M. Pu(IV) concentration in the carbonate medium was determined from the absorbance of the 486 nm peak for which the molar extinction coefficient is 66 L.mol-1.cm^{-1}.[39]

A 0.15 M solution of Th(IV) nitrate ($Th(NO_3)_4.5H_2O$, Sigma Aldrich) was dissolved in a 3 M carbonate solution to obtain a $Th(CO_3)_5^{6-}$ solution.

Transferrin complexes spectrophotometry

Absorption spectra were recorded over the wavelength region 260–1000 nm with a single beam *Agilent Cary 60 UV/Vis* spectrophotometer and using a small volume 10 mm pathlength quartz cuvette.

The plutonium transferrin complex was prepared by mixing 50 µL of $Pu(CO_3)_5^{6-}$ stock, [Pu] = $3 x10^{-3}$ M, with 250 µL of Tf in the buffered solution: $5x10^{-2}$ M MES + $1.5x10^{-1}$ M NaCl; pH 7.4 ± 0.1. An addition of 30 µL HNO_3 2 M followed by a 50 µL addition of the buffer solution maintained the pH at 7.4 ± 0.1. After tree centrifugal steps (12 000g; 6 minutes; 4°C) followed by rinsing with the buffer medium was carried out. The final volume is adjusted at 250 µL with a buffer solution. The different complexes were prepared using the same protocol. For samples containing DFOB, 25µL was added with an initial concentration of $3 x 10^{-3}$ M and another centrifugal step was performed (12 000g; 6 minutes; 4°C). The finals concentrations of samples analyzed by UV/Vis are about 3.10^{-6} M for and about 6.10^{-6} M for Pu.

Transferrin-Pu MD simulation

MD simulations were performed using AMBER 15 program package[48] with ff99SB force field applied on the protein. For Pu^{4+}, 12-6-4 LJ-type parameters developed by Merz et al. have been employed.[49] For carbonate ions, additional parameters were employed.[50] The starting structure was taken from Ce_2Tf (PDB:1FCK). Missing atoms including hydrogens were added and the protonation state of the protein was adjusted to mimic physiological pH (pH 7.4). Additional CO_3^{2-} as well as Na^+ ions were added to mimic the presence of bulk carbonate and to make the system electrostatically neutral. TIP3P waters were then added with a minimum water layer thickness of 10 Å. 500 steps of steepest descent and 500 steps of conjugate gradient with 500 kcal mol^{-1}Å^{-1} harmonic restraint on the protein was initially conducted after which 1000 steps of steepest descent and 1500 steps of conjugate gradient were performed without constraints. 40 ps of heating of the system from 0 to 298 K with 10 kcal mol^{-1} Å^{-1} harmonic restraint on the protein, after which another 1 ns preconditioning run was performed at 298 K without restraint on the solutes. Finally, 100 ns MD run was performed in a periodic boundary condition in the NPT ensemble at 298 K. Simulations were terminated and restarted every 5 ns to avoid artificial convergence to a particular geometry. The SHAKE algorithm, a 2 fs time integration step, 12 Å cutoff for non-bonded interactions, and the particle mesh Ewald (PME) method were used. MD trajectory was recorded at each 50 ps. Simulations were performed with different numbers of carbonate ions (0 to 3) bound to Pu. RMSD of all simulations are given in Figure S8 in SI of the Supporting Information.

Transferrin complexes IR spectroscopy

ATR-FTIR spectra were recorded on a Bruker Tensor 27 instrument by using a nitrogen cooled mercury cadmium telluride (MCT) detector. A six-reflection diamond crystal was used as the refection unit. 50 µL of each sample were put in a micro-volume cell placed directly on the crystal. Spectra were acquired with 4 cm^{-1} resolution and 1024 scans were averaged for each sample. The slit opening for the incident beam was optimized at 3 mm.

Fe, Th and Pu XAS measurements

XAS experiments were carried out on the MARS beamline at the SOLEIL synchrotron facility which is dedicated to the study of radioactive materials. The optics of the beamline consisted of a water-cooled double-crystal monochromator for incident energy selection and horizontal focalization, and two large water-cooled reflecting mirrors for high-energy rejection (harmonic part) and vertical collimation and focalization. All the measurements were recorded in double-layered solution cells (200µL) specifically designed for radioactive samples at room temperature. The calibration of the incident beam energy was performed at the K threshold jump of Yttrium corresponding to 17.038 keV. A specific cell was used for the radioactive samples and consisted of Teflon sample holders containing three 250 µL slots closed by two layers of Kapton® (polyimide) film on each side.

EXAFS data were acquired at the Th L_{III} edge (16 300 eV), at the Pu L_{III} edge (18 057 eV). Data were processed by using the ATHENA code of Demeter 0.9.25 package.[51] EXAFS data were adjusted using phases and amplitudes calculated with Feff7 code embedded in ARTEMIS code of Demeter 0.9.25. The site of Pu3(B) obtained in the above MD B calculations was used as a model. EXAFS signal was fitted in R space between 1 and 6 Å without any additional filtering after Fourier transformation using a Hanning window in k^2 (2.7 - 10.8 Å^{-1}). In all the fits, only one global amplitude factor S_0^2 and one energy threshold e_0 factor were considered for all the contributions. The agreement factor R (in %) and quality factor reduced χ^2 (Q) are both provided as an indication of the fit quality.

Simulation of the Pu sites of different models calculated by MD calculation were performed with Feff9 code.

Fe, Th and Pu SAXS measurements

SAXS experiments were subsequently performed with an X-ray energy of 16.0 keV corresponding to an average wavelength of 0.7749 Å-1, and a sample-to-detector distance of 763.67 mm. This configuration allows a Q range of approximately 0.02 Å-1 to 2 Å-1. A tank filled with He gas containing the centered photodiode beam stop was placed between the sample holder and the Pilatus 3 2M CdTe detector to reduce air diffusion.[52] Sample transmissions were recorded for 5 s using photodiodes and scattering patterns were recorded for 45 s per sample. The isotropic 2D scattering data were azimuthally averaged to obtain the scattering intensity I(Q) using the PyFAI software.[53] The scattering intensity of the samples was then normalized by acquisition time, transmission and thickness, and multiplied by a normalization constant determined using the scattering intensity of polyethylene (PE) at Q= 0.36 nm-1 which corresponds to 4.9 cm-1. The absolute intensity scattered by the samples was finally obtained by subtracting the contributions of the empty cells, the solvent and the background. The data was simulated using SasView 4.2.0 software. The solvent signal was subtracted, prior to fitting these spectra with an ellipsoid form factor.

Acknowledgements

All MD calculations were performed at Zentrum für Informationdienste und Hochleistungrechnen of Technische Universität Dresden, Germany. The generous allocation of computing time is gratefully appreciated.

XAS and SAXS data were collected at the MARS beam line of SOLEIL synchrotron, Saint-Aubin, France.

This work benefited from the use of the SasView application, originally developed under NSF award DMR-0520547. SasView contains code developed with funding from the European Union's Horizon 2020 research and innovation programme under the SINE2020 project, grant agreement No 654000.PhD fellowship of C. Zurita was provided by the Ministry of Higher Education and Research, France

Keywords

Metalloprotein, Plutonium, Transferrin, XAS, SAX

Supporting information file

3 sections provided :

1- Spectroscopy
2- MD simulation and EXAFS data analysis
3- SAXS measurements

1- Spectroscopy

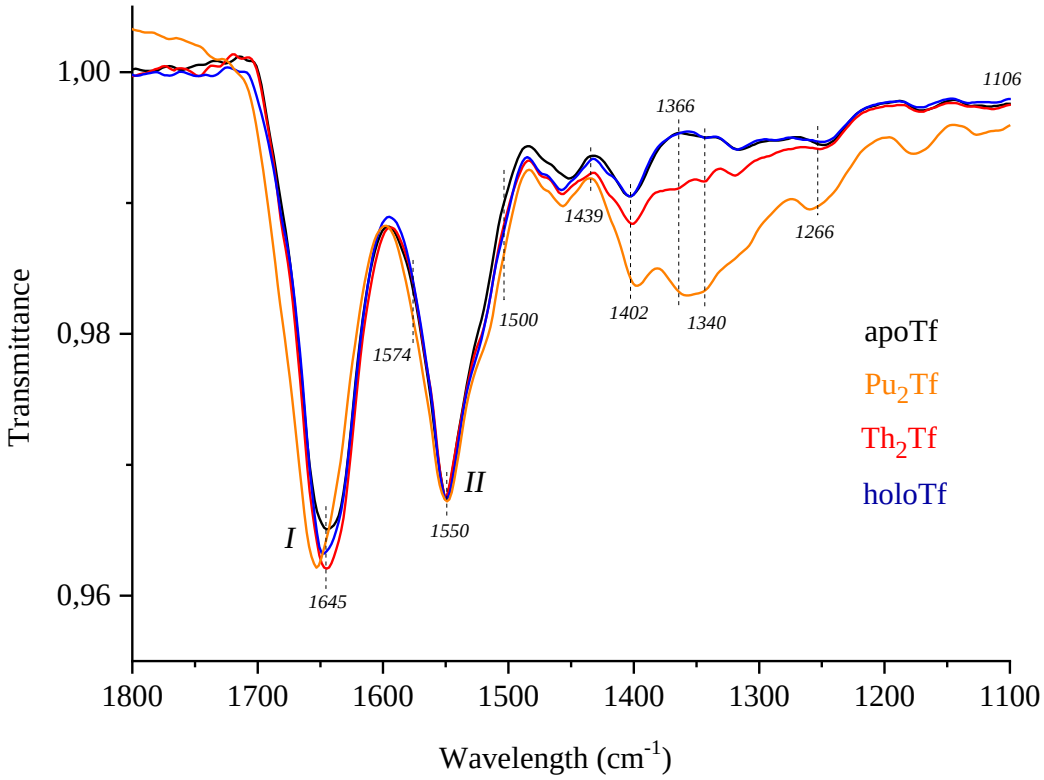

Figure S1: Comparison of the infrared spectra of Th_2Tf (red line), Pu_2Tf (orange line), holoTf (blue line), apoTf (black line) complexes. Spectra normalized in transmittance with respect to the characteristic band of amide I (1645 cm^{-1})

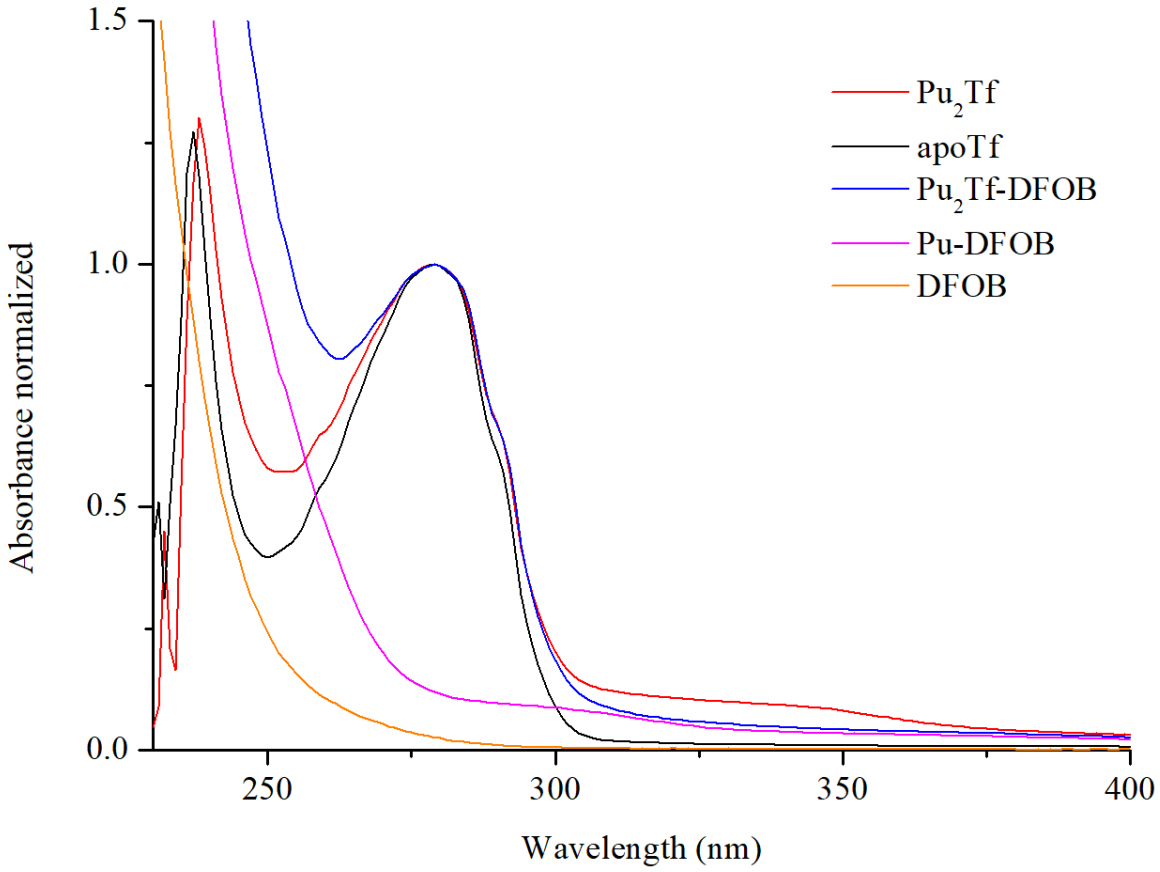

Figure S7: UV-Visible spectroscopy comparison of Pu_2Tf (red line), DFOB (orange line), Pu_2Tf-DFOB (blue line), Pu-DFOB (purple line) and apoTf (black line).

2- MD simulation and EXAFS data analysis

Model	Structure
$Pu_2Tf(1carb)$	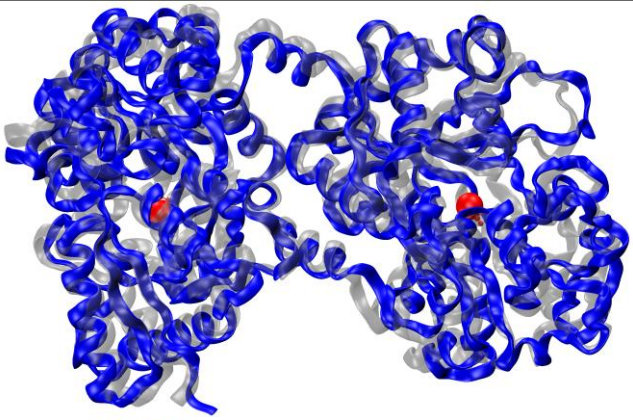
$Pu_2Tf(2carb)$	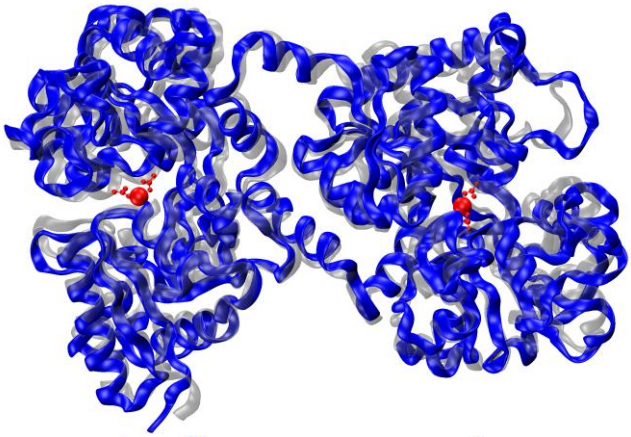
$Pu_2Tf(3carb)$	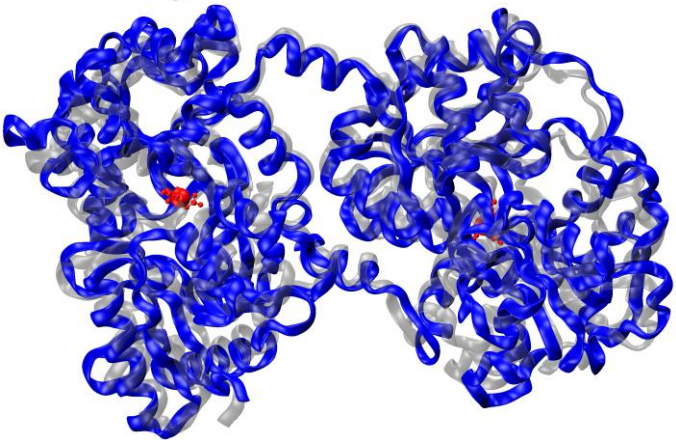

Figure S2: Superposition of the PDB structure: 1FCK (grey) with the three Pu_2Tf models (blue) calculated by molecular dynamics

Table S1: Local environments (number, type of ligand and amino acid of the protein) of Pu(IV) in the N and C lobes of the computed molecular dynamics simulations of Pu_2Tf (*1carb*) and Pu_2Tf (*2carb*) models (bi = bidentate interaction; mon = monodentate interaction; a.a = amino acid).

Pu_2Tf (1carb) :

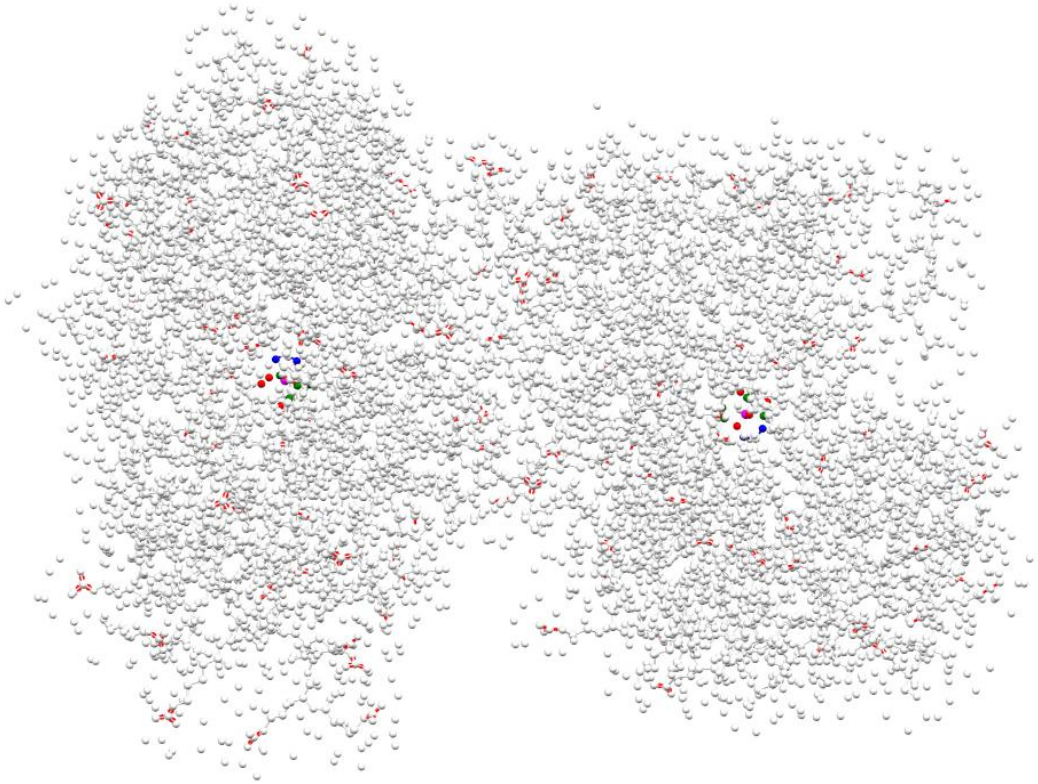

Pu_2Tf (2carb) :

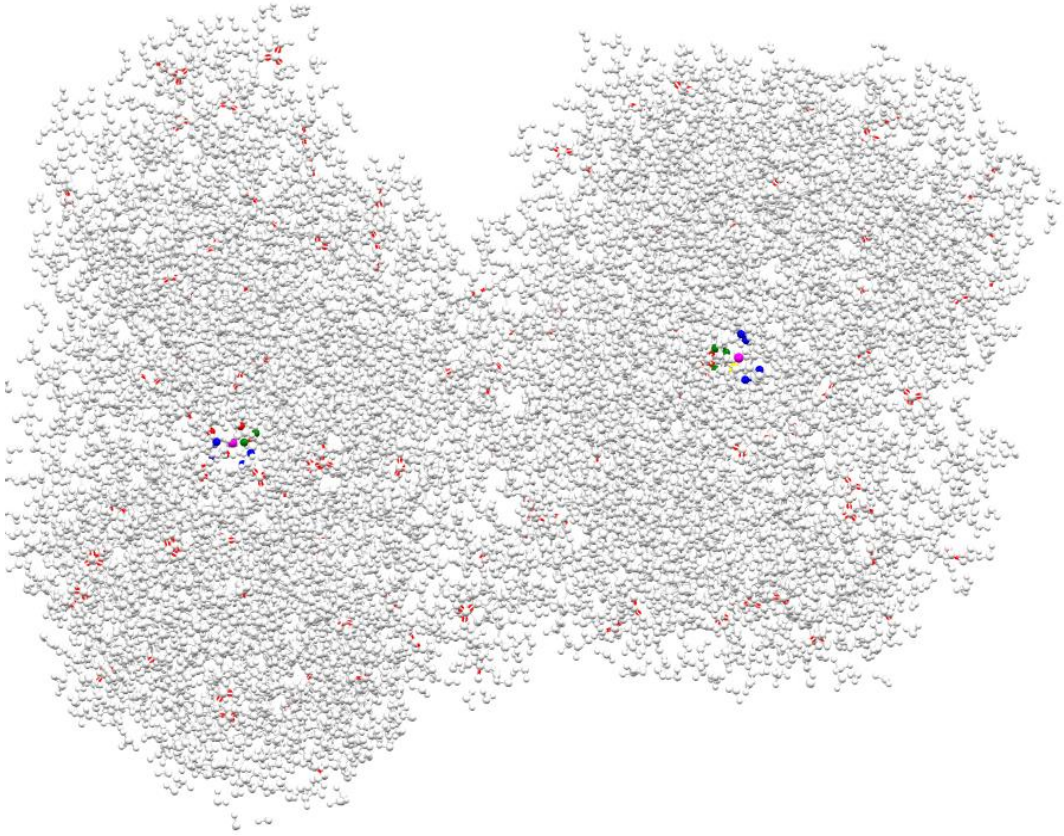

Model	**N-Lobe** a.a. sequence number	**C-Lobe** a.a. sequence number	**CN**	
Pu_2Tf (1carb)	1 Asp 60 (bi) 1 Carbonate (bi) 1 Glu 80 (mon) 1 Ser 252 (mon) 4 Water	1 Asp 395 (bi) 1 Carbonate (bi) 1 Ala 594 (mon) 1 Pro 595 (mon) 4 Water	N-Lobe (top): 10 (3 a.a) C-Lobe (bottom): 10 (3 a.a)	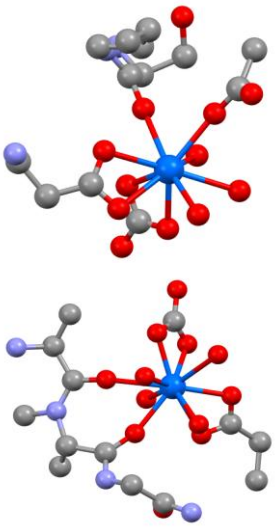

Pu_2Tf (2carb)	2 Carbonates (bi) 1 Asp 60 (mon) 4 Water	2 Carbonates (bi) 1 Asp 395 (bi) 1 Thr 466 (mon) 1 Water	N-Lobe (top): 9 (1 a.a) C-Lobe (bottom): 10 (2 a.a)	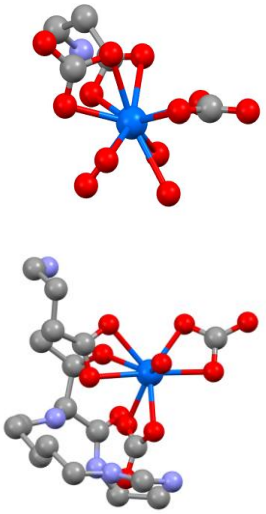
Fe_2Tf (PDB: 1N04)	1 Asp 60 (mon) 1 Carbonate (bi) 2 Tyr 92, 191 (mon) 1 His 250 (mon)	1 Asp 395 (mon) 1 Carbonate (bi) 2 Tyr 431, 524 (mon) 1 His 592 (mon)	6 (4 a.a)	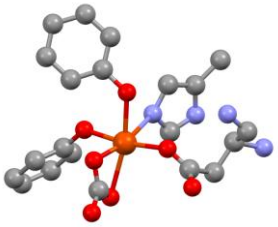
Ce2Tf (PDB: 1FCK)	1 Asp 60 (mon) 1 Carbonate (bi) 2 Tyr 92, 192 (mon) 1 His 253 (mon)	1 Asp 395 (mon) 1 Carbonate (bi) 2 Tyr 435, 528 (mon) 1 His 597 (mon)	6 (4 a.a)	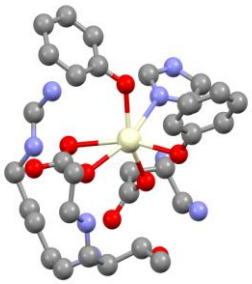

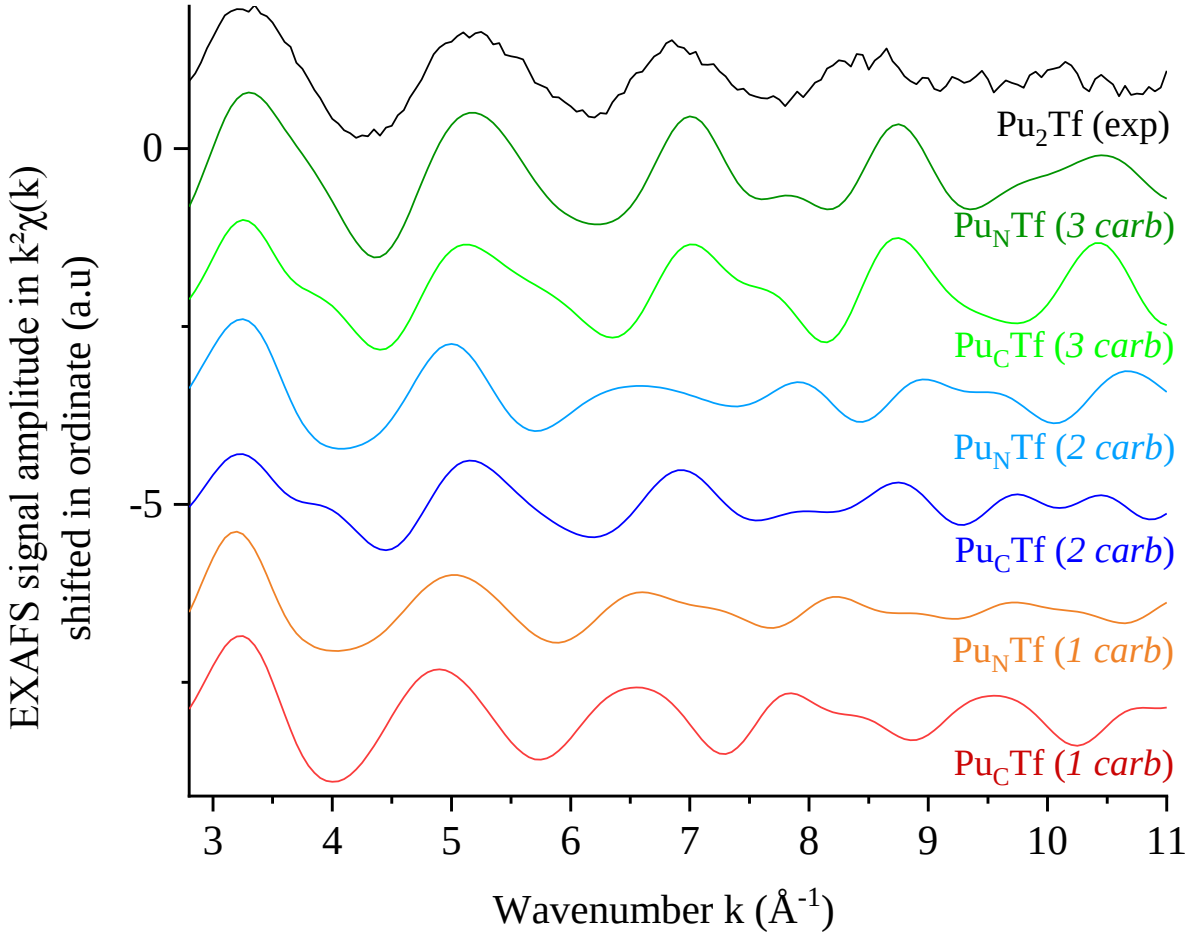

Figure S3: Theoretical EXAFS spectra of N and C lobe of each model along with experimental spectrum.

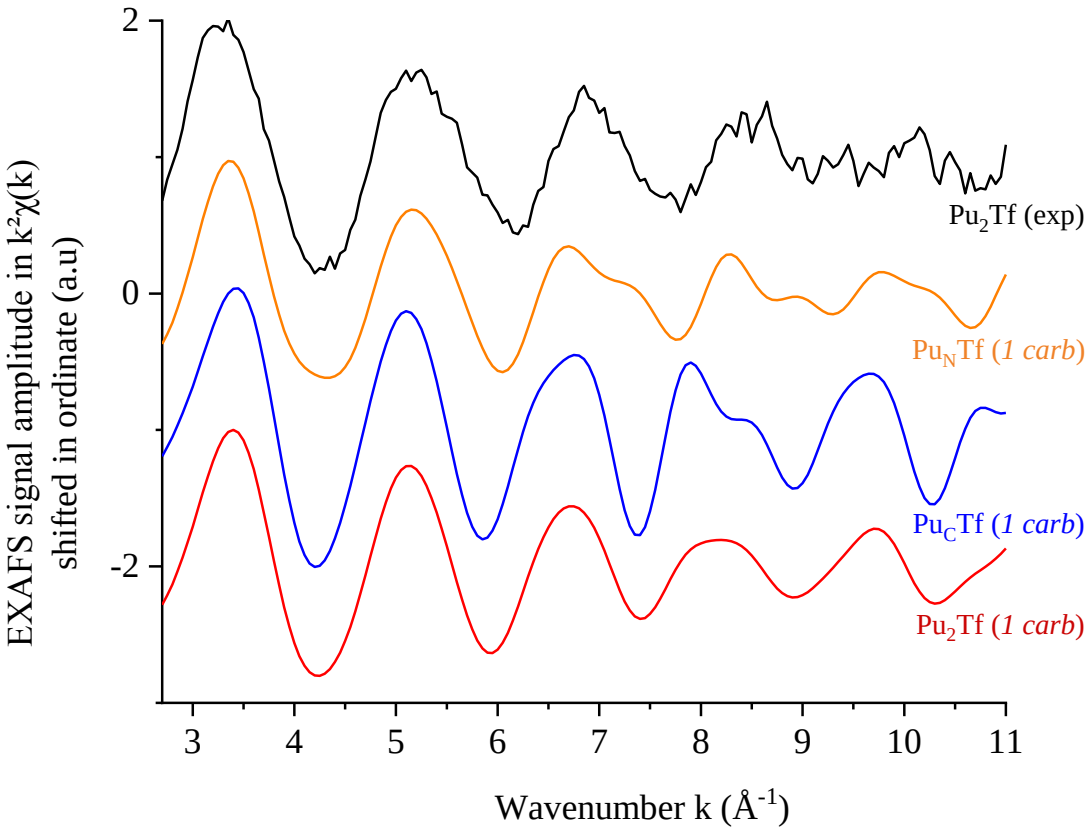

Figure S4: Comparison of theoretical EXAFS spectra in $k^2\chi(k)$ of the two lobes N and C (orange and blue line respectively) of the Pu_2Tf (*1carb*) complex model with the experimental spectrum of the Pu_2Tf complex (black line) and the average Pu_2Tf (*1carb*) model (red line)

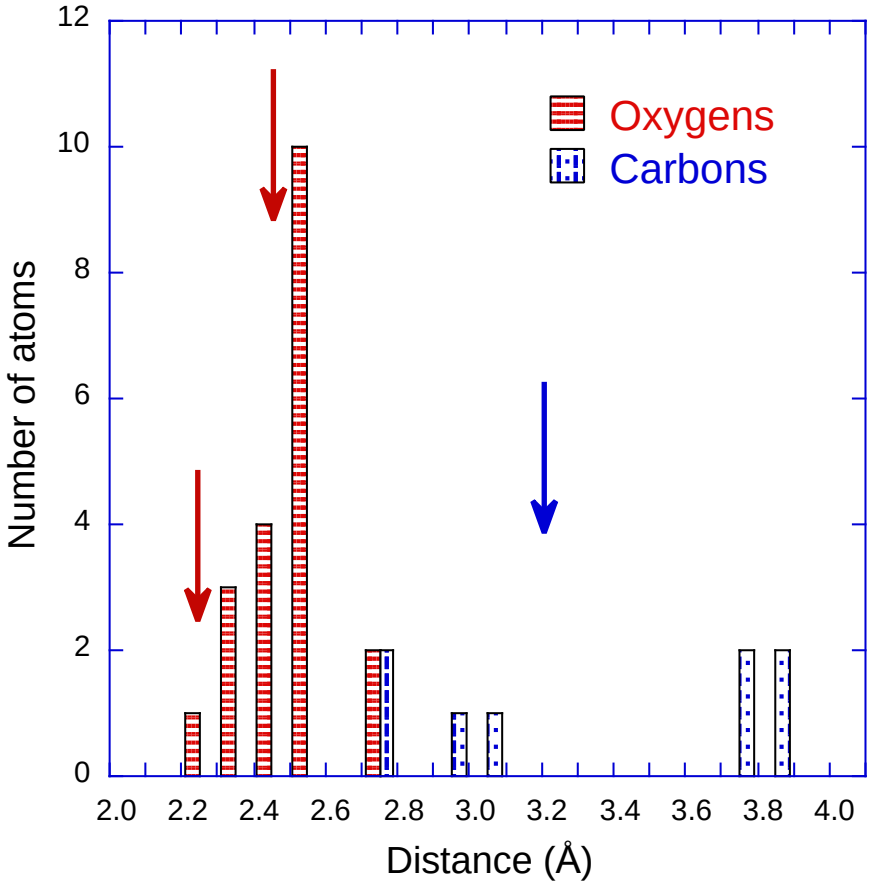

Figure S5: Frequency diagram of the Pu…X distances (X = O, C) in the PuTf(1carb) model considering intervals of 0.1 Å. Both lobes N and C have been considered. Oxygens are in red, ad carbon are in blue. Only atoms at distance < 4 Å from Pu have been represented. H have been omitted. Vertical arrows are representing the EXAFS best fit distances for Pu-O and Pu…C.

A

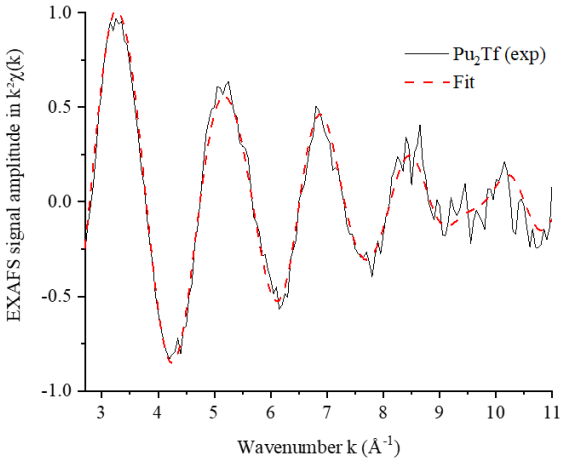

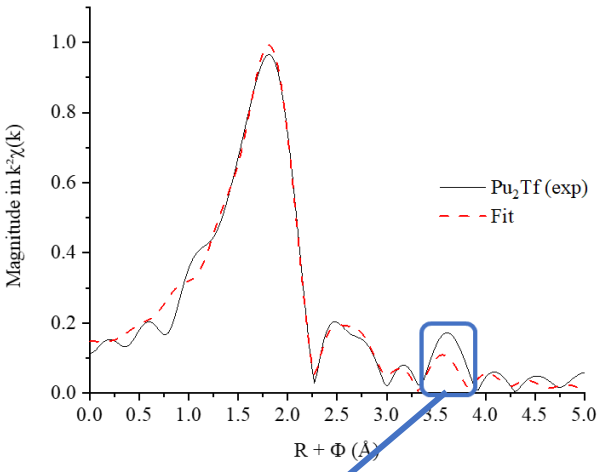

Fit with O distal contribution

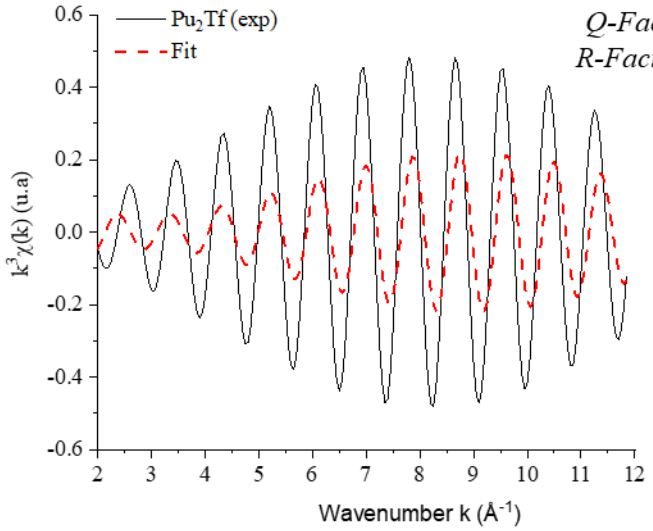

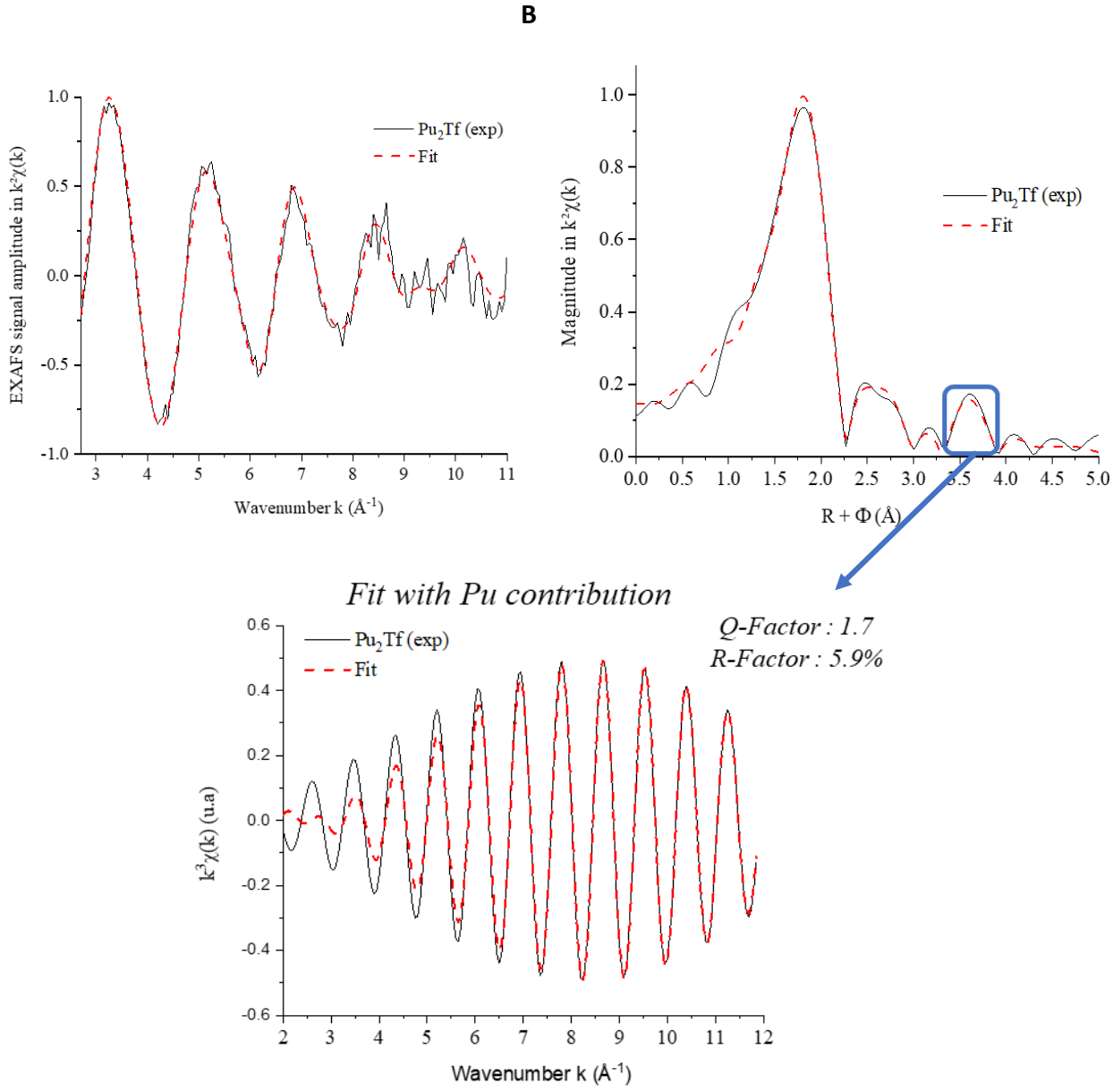

Figure S6: A) Experimental EXAFS spectrum filtered between R+Φ = 3.32 Å and 3.91 Å of the Pu_2Tf (exp) complex sample (solid line in black) and its fit (red dashed) with the distal oxygen contribution; B) Experimental EXAFS spectrum filtered between R+Φ = 3.32 Å and 3.91 Å of the Pu_2Tf (exp) complex sample (solid line in black) and its fit (dashed red) with the Pu-Pu contribution.

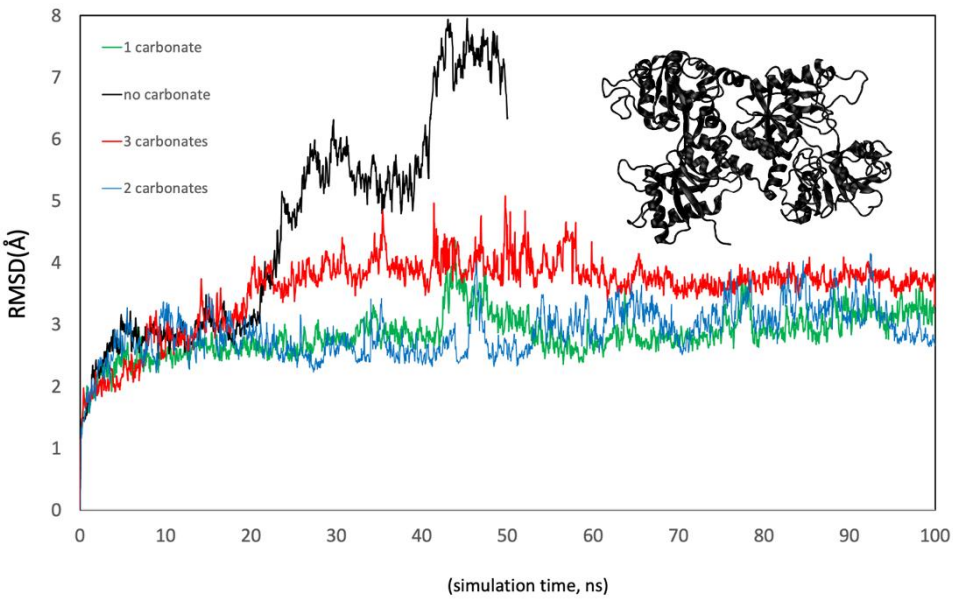

Figure S8: RMSD (Root-mean square deviation) of atomic positions of four independent MD simulations with different number of carbonate ions bound to Pu. Large fluctuations as seen in the simulation without carbonate (black line) suggest that the structure gets distorted when carbonate ion is absent. The structure of Pu_2Tf without carbonate at t = 50 ns (right top) shows that the binding pocket fully opens during the simulation and Pu get easily "excreted". Proteins in simulations with 1 to 3 carbonates remain folded and show overall stability.

3- SAXS measurements

Firstly, a statistical study was carried out, measuring each complex ten times, in order to calculate a mean spectrum and standard deviation and to check that the samples have not been damaged by the beam. The buffer medium used to make the complexes and the empty cells were analyzed under the same conditions. For all the samples analyzed, the average relative standard deviation between spectra is less than 3% except for the Pu_2Tf n°2 (4.57%) and Th_2Tf n°1 (34.50%) measurements (see Table 4 of SI). Beyond a probable variation of the beam intensity over the measurement, this problem seems to be due to the data flow transfer, linked to the repetition of short acquisitions and the real time of responses between the different devices of the beamline. For Th_2Tf n°1, the coefficient of mean variation is reduced from 34.50% to 2.17% by omitting the divergent spectrum measurement. If degradation was the cause of this large variation, large mean coefficients of variation would have been observed for all consecutive measurements. Overall, the acquisition of the spectra for the same sample is repeatable and shows that the protein was not damaged under the beam as the calculated deviations are similar to those observed in our buffer medium alone and in the empty cells.

Table S2: Average relative standard deviation, in percent, of the ten recorded spectra for each sample.

Sample	Relative standard deviation (%)
Empty tube n°1	1.99 ± 0.01
Empty tube n°2	1.66 ± 0.01
Buffer n°1	1.99 ± 0.01
Buffer n°2	1.29 ± 0.01
Pu_2Tf n°1	2.22 ± 0.01
Pu_2Tf n°2	4.57 ± 0.01
Pu_2Tf n°3	2.12 ± 0.01
Pu_2Tf-DFOB	1.85 ± 0.01
Th_2Tf n°1	34.50 ± 0.25 / 2.12 ± 0.01 (*after removal of the different spectrum*)
Th_2Tf n°2	2.25 ± 0.01
Th_2Tf n°3	2.86 ± 0.01
Th_2Tf-DFOB	1.82 ± 0.01
holoTf n°1	1.25 ± 0.01
holoTf n°2	1.55 ± 0.01
holoTf-DFOB	1.45 ± 0.01
apoTf n°1	1.44 ± 0.01
apoTf n°2	1.81 ± 0.01
apoTf n°3	1.50 ± 0.01

The average spectrum, at each point, of the different samples is calculated according to the formula:

$$m = \frac{1}{n}\sum_{i=1}^{n} x_i$$

Then the variance, which represents the dispersion of the values of a sample, was calculated, at each point, of the different samples according to the formula:

$$V = \frac{1}{n}\sum_{i=1}^{n} (x_i - m)^2$$

The standard deviation is deduced from the variance, at each point, according to the formula:

$$\sigma = \sqrt{V}$$

Finally, the relative standard deviation, noted RSD, was calculated, at each point, according to the formula:

$$RSD = \frac{\sigma}{m}$$

Table S3: Guinier fitting approximation of the SAXS data of apoTf, holoTf, M_2Tf, holoTf-DFOB and M_2Tf-DFOB complexes (M = Th(IV), Pu(IV); pH ~ 7.4; I = 0.05 M), this work, using SASView© software. χ^2 represents the error of fit. Comparison with the radius of gyration (in Å) calculated from MD model of Pu_2Tf with 1,2 or 3 carbonates. Comparison also with the radius of gyration (in Å) of Yajima et al.[43], Jensen et al.[16]

Sample	**Rg (Å)**	**Fitting error χ^2**	MD models	Yajima et al.	Jensen et al.
apoTf	28.7 ± 0.1	$3.3.10^{-5}$		30.3	
Th_2Tf	28.9 ± 0.3	$4.7.10^{-6}$			
Pu_2Tf	28.8 ± 0.2	$1.7.10^{-5}$	30.1 ± 0.2 (1carb) 30.4 ± 0.1 (2carb)		34.2± 0.6
holoTf	27.6 ± 0.1	$3.9.10^{-5}$		29.3	33.2
Th_2Tf-DFOB	30.5 ± 0.3	$7.3.10^{-7}$			
Pu_2Tf-DFOB	30.4 ± 0.2	$3.6.10^{-6}$			
holoTf-DFOB	30.3 ± 0.2	$9.9.10^{-7}$			

[1] National Council on Radiation Protection and Measurements. *Management of persons contaminated with radionuclides.* vol. 1,2008.
[2] A. E. V. Gorden, J. Xu, K. N. Raymond, P. Durbin, *Chem. Rev.* **2003**, *103*, 4207-4282.
[3] G. R. Choppin, *Rad. Chim. Acta*. **1983**, *32*, 43-54.
[4] L. R. Morse, N. M. Edelstein, J. Fuger, J.J. Katz, *The chemistry of the actinide and transactinide elements*. Ed. Springer, **2006**.
[5] P.W. Durbin, *Health Phys.* **1962**, *8*, 665-671.
[6] B. Ramounet, S. Matton, G. Grillon, P. Fritsch, *J. Alloys Compd.* **1998**, *271–273*, 103-105.
[7] ICRP publication n°56. *Age-dependent doses to members of the public from intake of radionuclides. 1*., Pergamon Press, **1990**.
[8] S.A. Romanov, A.V. Efimov, E.E. Aladova, K. G. Suslova, I.S. Kuznetsova, A.B. Sokolova, V.V. Khokhryakov, S.A. Sypko, M.V. Ishunina, V.F. Khokhryakov, *J. Environ. Radioact*. **2020**, *211*, 106073.
[9] A. Van Der Meeren, O. Gremy, D. Renault A. Miroux, S. Bruel, N. Griffiths, F. Tourdes, *J. Rad. Res.* **2012**, *53*, 184-194.
[10] R.D. Shannon, *Acta Cryst*. **1976**, *A32*, 751-767.
[11] M.L. Kennard, D.R. Richardson, R. Gabathuler, P. Ponka, W.A. Jefferies, *EMBO J.* **1995**, *14*, 4178-4186.
[12] S. Vaulont, *Arch. Pédiatrie* **2017**, *24*, 5S32-5S39.
[13] G. Boocock, C.J. Danpure, D.S. Popplewell, D.M. Taylor, *Radiat. Res.* **1970**, *42*, 381-396.
[14] D.M. Taylor, *J. Alloys Compd*. **1998**, *271–273*, 6-10.
[15] J.R. Duffield, D.M. Taylor, S.A. Proctor, *Int. J. Nucl. Med. Biol.* **1986**, *12*, 483-487.
[16] M.P. Jensen, D. Gorman-Lewis, B. Aryal, T. Paunesku, S. Vogt, P.G. Rickert, S. Seifert, B. Lai, G.E. Woloschak, L. Soderholm, *Nat. Chem. Biol.* **2011**, *7*, 560-565.
[17] P. Aisen, A. Leibman, J. Zweier, *J. Biol. Chem.* **1978**, *253*, 1930-1937.
[18] H.A. Huebers, C.A. Finch, *Physiol. Rev.* **1987**, *67*, 520-582.
[19] J. Wally, P.J. Halbrooks, C. Vonrhein, M.A. Rould, S.J. Everse, A.B. Mason, S.K. Buchanan, *J. Biol. Chem.* **2006**, *281*, 24934-24944.
[20] P. Aisen, *Int. J. Biochem. Cell Biol.* **2001**, *33*, 940-959.
[21] P.T. Gomme, K.B. McCann, J. Bertolini, *Drug Discov. Today* **2005**, *10*, 267-273.
[22] H. Sun, H. Li, P.J. Sadler, *Chem. Rev.* **1999**, *99*, 2817-2842.
[23] J. Williams, K. Moreton, *Biochem. J.* **1980**, *185*, 483-488.
[24] E.N. Baker, *Advances in Inorganic Chemistry* Ed. Elsevier **1994**, *41* 389-463.
[25] P.J. Sargent, S. Farnaud, R.W. Evans, *Curr. Med. Chem.* **2005**, *12*, 2683-2693.
[26] P. Aisen, R. Aasa, B.G. Malmström, T. Vänngård, *J. Biol. Chem.* **1967**, *242*, 2484-2490.
[27] Y. Cheng, O. Zak, P. Aisen, S.C. Harrison, T. Walz, *Cell* **2004**, *116*, 565-576.
[28] J.B. Vincent, S. Love, *Biochim. Biophys. Acta - Gen. Subj.* **2012**, *1820*, 362-378.
[29] S. Sauge-Merle, D. Lemaire, R.W. Evans, C. Berthomieu, J. Aupiais, *Dalton Trans.* **2017**, *46*, 1389-1396.
[30] P.K. Bali, W.R. Harris, *Arch. Biochem. Biophys.* **1990**, *281*, 251-256.
[31] H.H. Cai, J. Cai, P.H. Yang, *Bioorg. Med. Chem. Lett.* **2009**, *19*, 863-866.
[32] M.S. Shongwe, R. Smith, H.M. Marques, J.A. van Wyk, *J. Inorg. Biochem.* **2004**, *98*, 199-208.
[33] J.R. Duffield, D.M. Taylor, *Inorg. Chem. Acta*, **1987**, *140*, 365-367.
[34] W.R. Harris, C.J. Carrano, V.L. Pecoraro, K.N. Raymond, *J. Am. Chem. Soc*. **1981**, *103*, 2231-2237.
35 C. Vidaud, S. Gourion-Arsiquaud, F. Rollin-Genetet, C. Torne-Celer, S. Plantevin, O. Pible, C. Berthomieu, E. Quéméneur, *Biochemistry* **2007**, *46*, 2215-2226.
[36] H.M. Baker, C.J. Baker, C.A. Smith, E.N. Baker, *J. Biol. Inorg. Chem.* **2000**, *5*, 692-698.
[37] E.N. Baker, P.F. Lindley, *J. Inorg. Biochem.* **1992**, *47*, 147-160.
[38] D. Rinaldo, M.J. Field, *Biophys. J.* **2003**, *85*, P3485-3501.
[39] C. Zurita, S. Tsushima, C. Bresson, M. Garcia Cortes, P. Lorenzo Solari, A. Jeanson, G. Creff, C. Den Auwer, *Chem. Eur. J.* **2021**, *27*, 2393-2401.
[40] C. Ekberg, K. Larsson, G. Skarnemark, A. Ödegaard-Jensen, I. Persson, I. *Dalton Trans* **2013**, *42*, 2035-2040.
[41] A. Evers, R.D. Hancock, A.E. Martell, R.J. Motekaitis, *Inorg. Chem.* **1989**, *28*, 2189-2195.
[42] H. Boukhalfa, S.D. Reilly, M.P. Neu, *Inorg. Chem*. **2007**, *46*, 1018-1026.
[43] H. Yajima, H. Yamamoto, M. Nagaoka, K. Nakazato, T. Ishii, N. Niimura, *Biochim. Biophys. Acta - Gen. Subj*. **1998**, *1381*, 68–76.
[44] D. Bellotti, M. Remelli, *Molecules* **2021**, *26*, 3255.
[45] P. Martel, S.M. Kim, B.M. Powell, *Biophys. J.* **1980**, *31*, 371-380.
[46] A. Jeanson, M. Ferrand, H. Funke, C. Hennig, P. Moisy, P. Lorenzo Solari, C. Vidaud C. Den Auwer, *Chem. Eur. J.* **2010**, *16*, 1378-1387.
[47] C. Micheau, M. Virot, S. Dourdain, T. Dumas, D. Menut, P. Lorenzo Solari, L. Venault, O. Diat, P. Moisy, S.I. Nikitenko, *Environ. Sci. Nano* **2020**, *7*, 2252–2266.
[48] D.A. Case, I.Y. Ben-Shalom, S.R. Brozell, D.S. Cerutti, T.E. Cheatham III, V.W.D. Cruzeiro, P.A. Kollman, P. A. Amber 2015, University of California, San Francisco, USA, **2015**.
[49] P. Li, L.F. Song, K.M. Merz, *J. Phys. Chem. B* **2015**, *119*, 883-895.
[50] S. Kerisit, C. Liu, *Environ. Sci. Technol.* **2014**, *48*, 3899-3907.
[51] B. Ravel, M. Newville, *J. Synchrotron Radiat.* **2005**, *12*, 537-541.
[52] T. Dumas, M. Virot, D. Menut, C. Tamain, C. Micheau, S. Dourdain, O. Diat, *J. Synchrotron Radiat.* **2022**, *29*, 30-36.

[53] G. Ashiotis, A. Deschildre, Z. Nawaz, J.P. Wright, D. Karkoulis, F.E. Picca J. Kieffer, *J. Appl. Crystallogr*. **2015**, *48*, 510-519.